

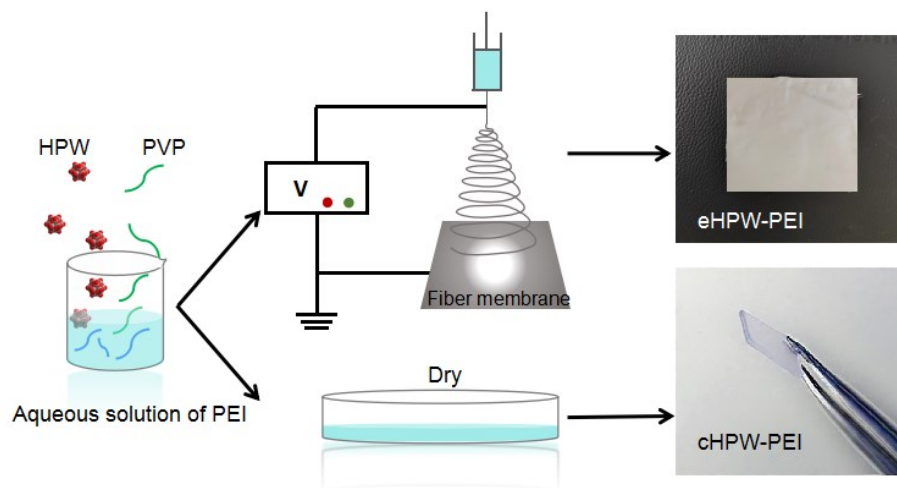
Supporting Information

‘Proton Escalator’ PEI and Phosphotungstic Acid Constructing a Nanofiber Membrane with Remarkable Proton Conductivity

Xiuwei Sun,^a Shumei Liu,^a Qingyin Wu,^{*b} Shan Zhang,^a Hongrui Tian,^a Xue Bai,^a
Zhuo Li,^a Ying Lu^{*a} and Shuxia Liu^{*a}□

*^aKey Laboratory of Polyoxometalate and Reticular Material Chemistry of Ministry of
Education, College of Chemistry, Northeast Normal University, Changchun, Jilin
130024, P. R. China. Email: liusx@nenu.edu.cn; luy968@nenu.edu.cn*

*^bDepartment of Chemistry, Zhejiang University, Hangzhou 310027, PR China. Email:
qywu@zju.edu.cn*



Scheme S1 Schematic diagram of preparation process of electrospinning membrane (eHPW-PEI) and casting membrane (cHPW-PEI).

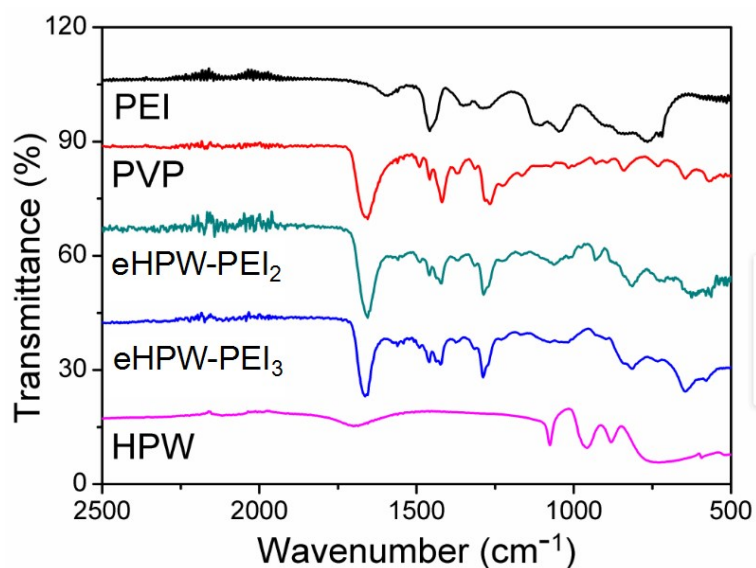


Fig. S1 FT-IR spectra of PEI, PVP, eHPW-PEI₂, eHPW-PEI₃ and HPW.

Fourier transform infrared (FT-IR) was used to confirm the successful synthesis of eHPW-PEI₂ and eHPW-PEI₃. As shown in Figure S1, the FT-IR spectra of eHPW-PEI₂ and eHPW-PEI₃ show the characteristic bands of [PW₁₂O₄₀]³⁻ Keggin structure at 1071 cm⁻¹ (P-O), 969 cm⁻¹ (W=Ot), 880 cm⁻¹ (W=Ob=W) and 768 cm⁻¹ (W=Oc=W). The bands of W=Ot has a blue shift phenomenon because of the H-bonds formed by O atoms and H atoms on PEI. It shows that HPW has been successfully introduced into the membrane and maintains the original Keggin structure.

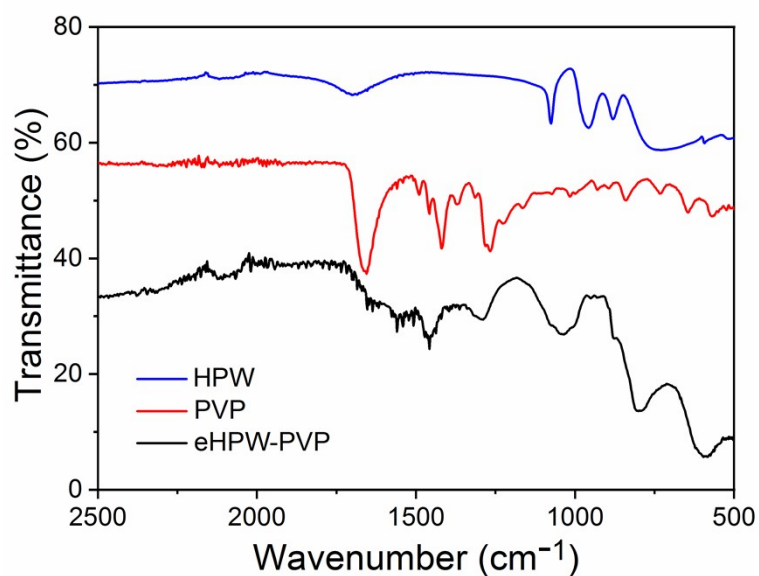


Fig. S2 FT-IR spectra of PVP, eHPW-PVP and HPW.

Fourier transform infrared (FT-IR) was used to confirm the successful synthesis of eHPW-PVP. As shown in Fig. S2, the FT-IR spectra of eHPW-PVP show the characteristic bands of $[\text{PW}_{12}\text{O}_{40}]^{3-}$ Keggin structure at 1076 cm^{-1} (P-O), 972 cm^{-1} (W=Ot), 888 cm^{-1} (W=Ob=W) and 766 cm^{-1} (W=Oc=W). It shows that HPW has been successfully introduced into the membrane and maintains the original Keggin structure.

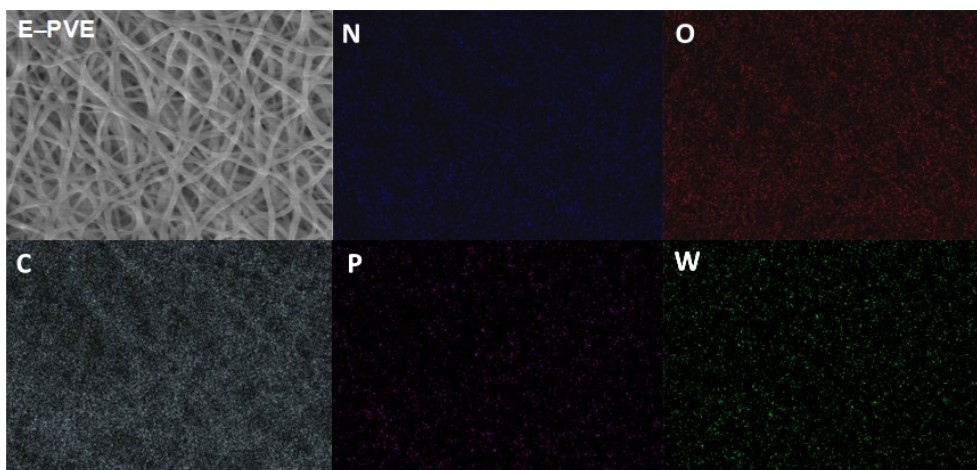


Fig. S3 Elemental mapping for eHPW-PEI₁, N (blue), O (red), C (gray), P (pink), W (green).

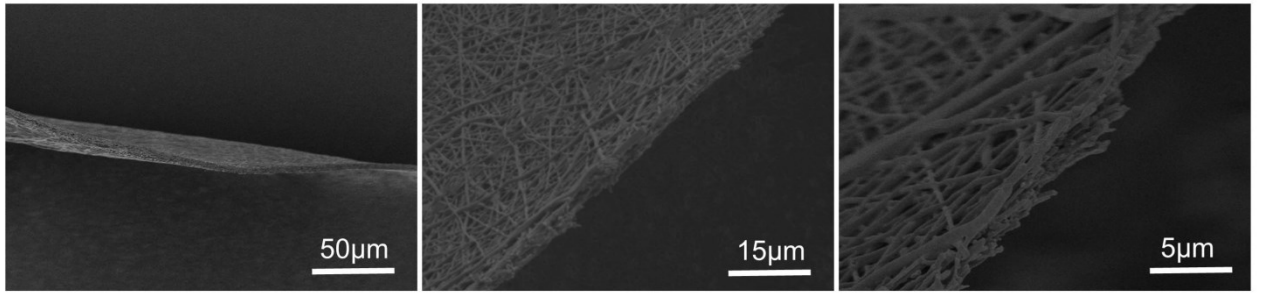


Fig. S4 SEM images of eHPW-PEI's cross section.

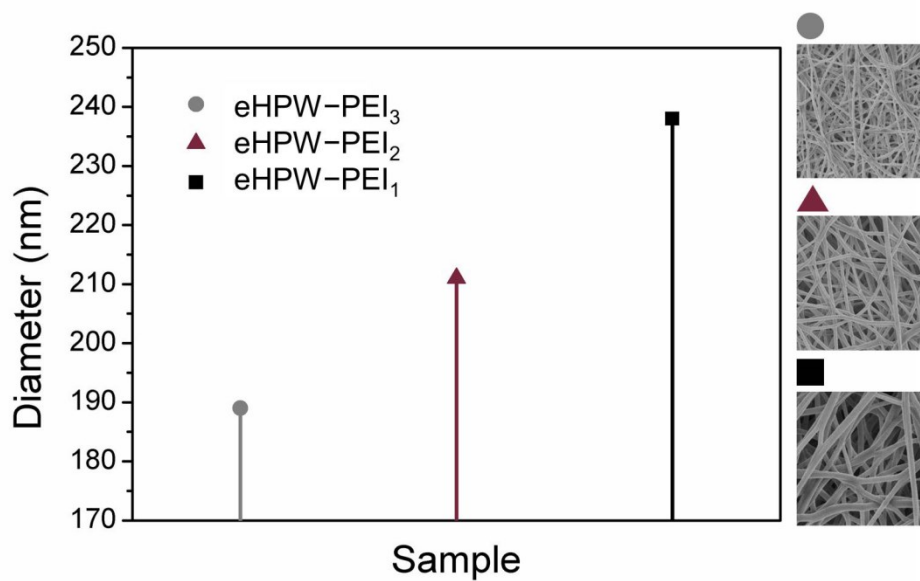


Fig. S5 Nanofibers average diameter and SEM images of eHPW-PEI₁, eHPW-PEI₂ and eHPW-PEI₃.

The eHPW-PEI₁, eHPW-PEI₂ and eHPW-PEI₃ membranes were morphologically characterized by SEM experiment. As shown in Figure S5, the nanofibers all have a uniform fiber structure and fiber diameter became larger with increasing of HPW wt% because more HPW lead to the higher conductivity of the spinning solution.

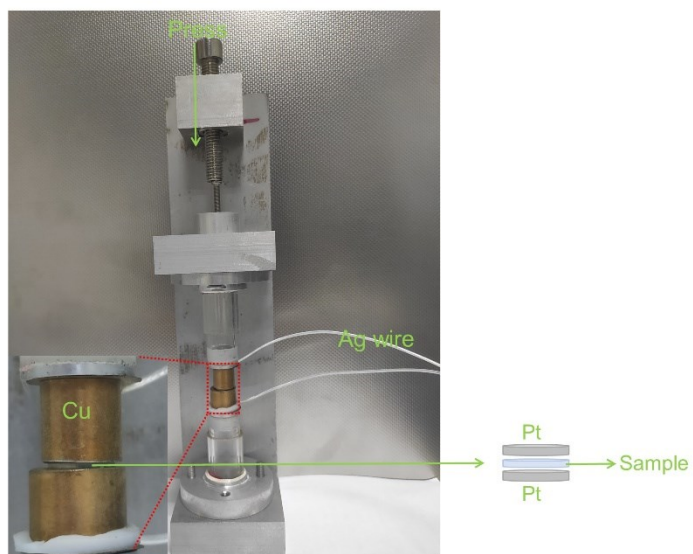


Fig. S6 Self-made electrodes and fixtures.

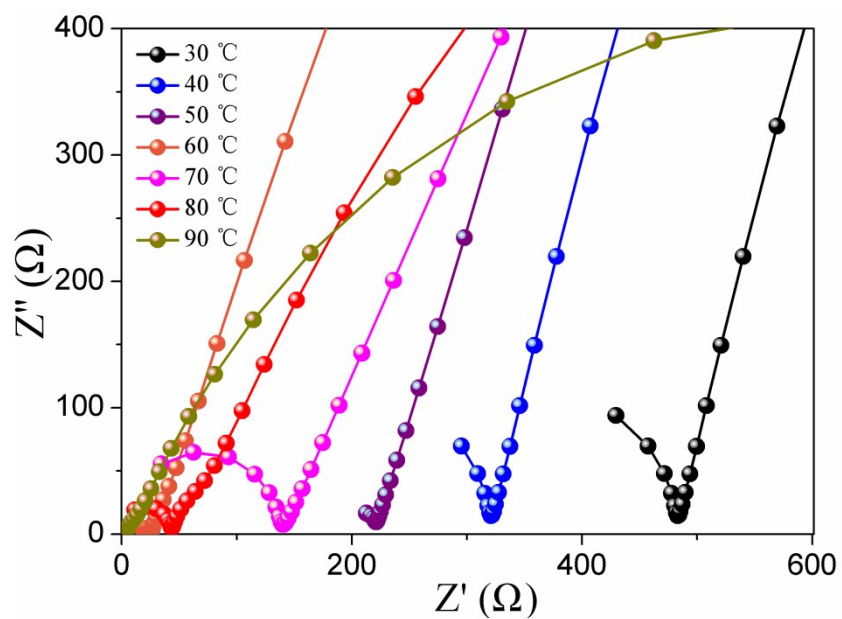


Fig. S7 Typical Nyquist plots at different temperatures for eHPW-PEI₁ under 90% RH.

Typical Nyquist plots of eHPW-PEI₁ under 90% RH are shown in Figure S7. We calculated that the proton conductivity of eHPW-PEI₁ reached to 0.03 S cm⁻¹ at 85 °C, 90% RH.

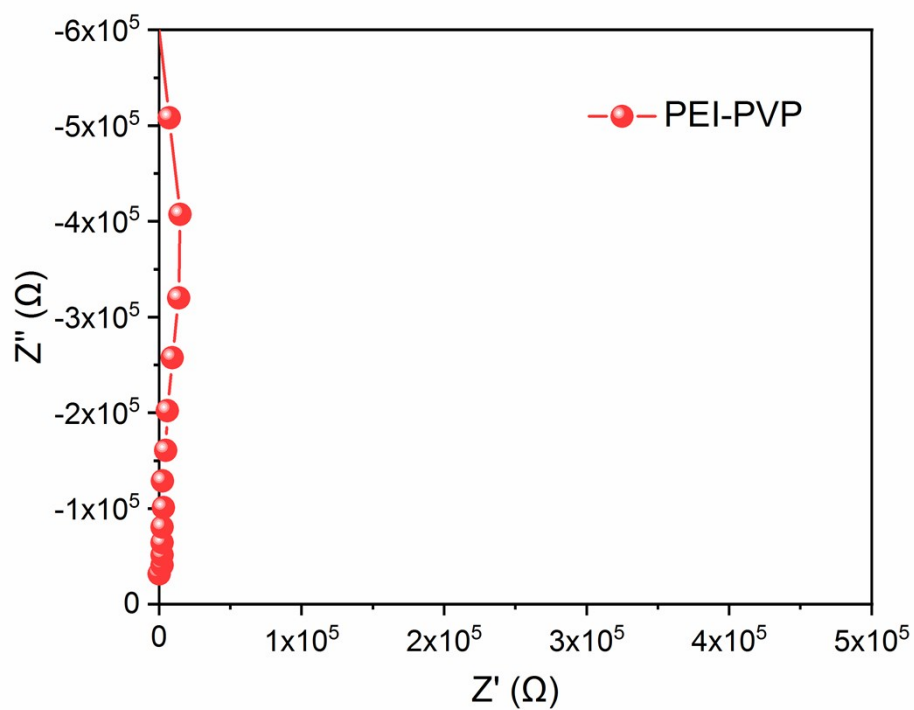


Fig. S8 Typical Nyquist plots at different temperatures for PEI–PVP under 85 °C, 90% RH.

PEI–PVP's proton conductivity is extremely low, its resistance is beyond the range of the instrument. This result indicates that HPW is the sole proton provider.

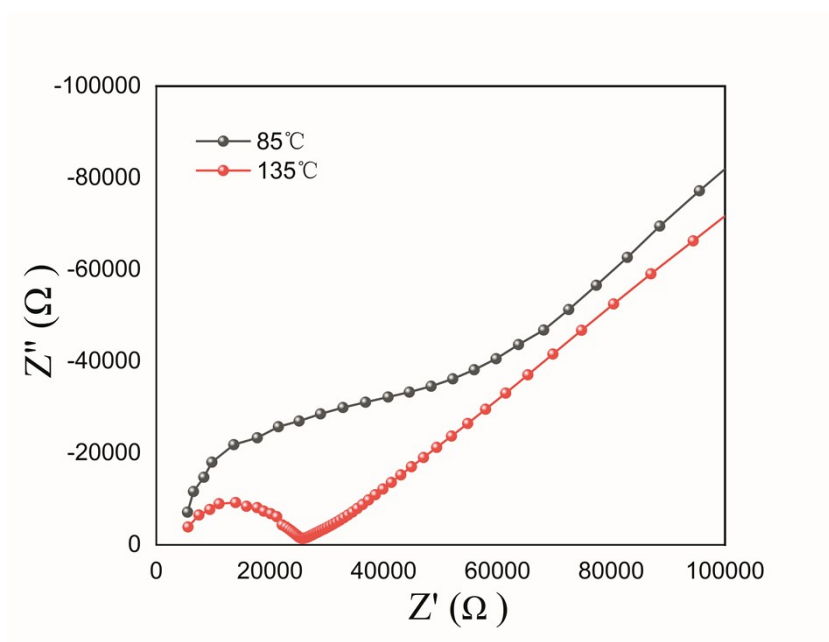


Fig. S9 Typical Nyquist plots of eHPW-PEI₁ at 85°C with 60% RH (black) and 135°C, without RH (red).

We conducted an AC impedance test on the membrane through-plane and calculated the proton conductivity according to the Nyquist plots (Fig. S9). The proton conductivity of eHPW-PEI₁ in-plane ($1.7 \times 10^{-3} \text{ S cm}^{-1}$ at 85 °C and 60% RH and $3.8 \times 10^{-3} \text{ S cm}^{-1}$ at 135°C) is slightly higher than through-plane ($1.6 \times 10^{-3} \text{ S cm}^{-1}$ at 85 °C with 60% RH and $3.7 \times 10^{-3} \text{ S cm}^{-1}$ at 135°C). This is due to the fact that the orientation of the fibers is consistent with the direction in which the membrane stretches, and it has a more continuous and convenient proton transmission path. The difference in proton conductivity along the two directions is not large, which increases the possibility of its practical application, because in most devices, protons are transported in the direction perpendicular to the membrane.

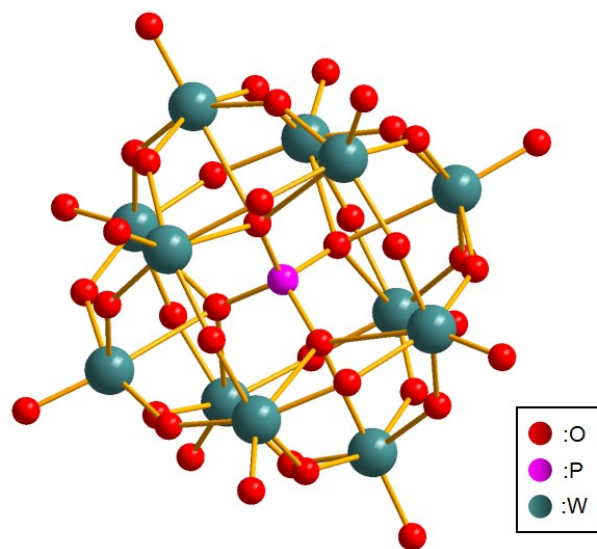


Fig. S10 The single crystal structure of HPW.

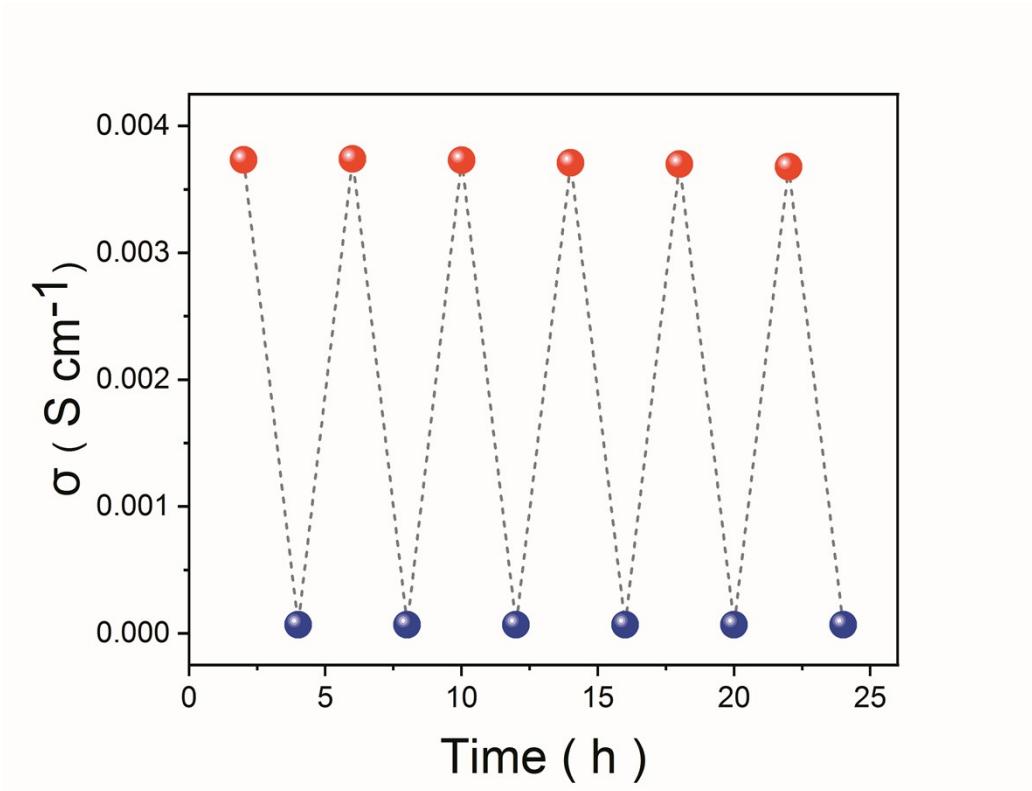


Fig. S11 The eHPW-PEI₁'s anhydrous proton conductivity diagram of the heating and cooling (red: 135°C, blue:25°C).

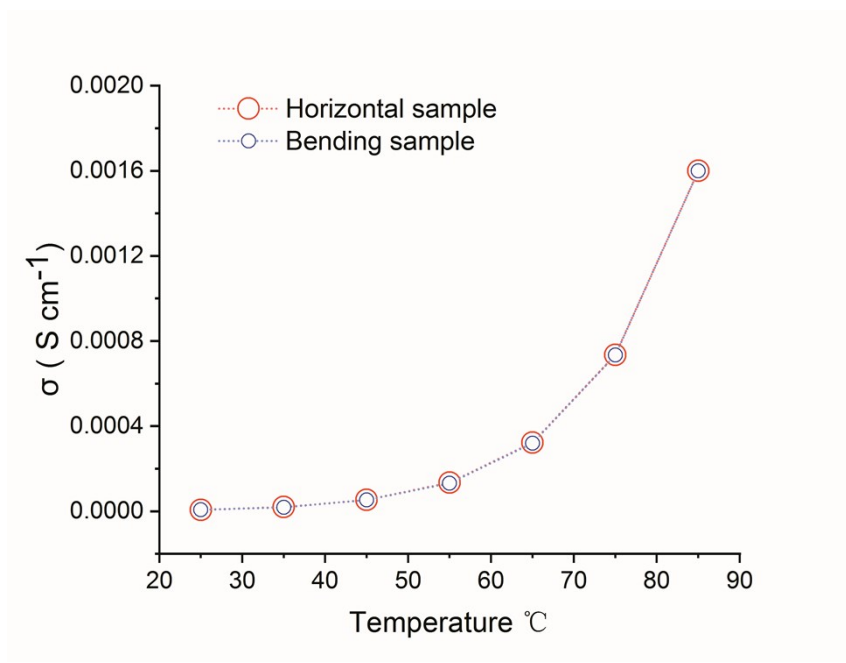


Fig. S12 The proton conductivity of the curved sample and the horizontal membrane of eHPW-PEI₁.

We conducted an AC impedance test on the bent eHPW-PEI₁ at different temperatures of 60 RH%, and calculated the proton conductivity of the sample according to the Nyquist diagram. The proton conductivity of the curved sample and the horizontal membrane of eHPW-PEI₁ are shown in the Fig. S12. We found that the proton conductivity of eHPW-PEI₁ in the two different states is almost the same, which indicates that the proton conductivity of eHPW-PEI₁ will not be affected by the shape of the membrane, which is mainly due to the high flexibility of the eHPW-PEI₁ membrane.

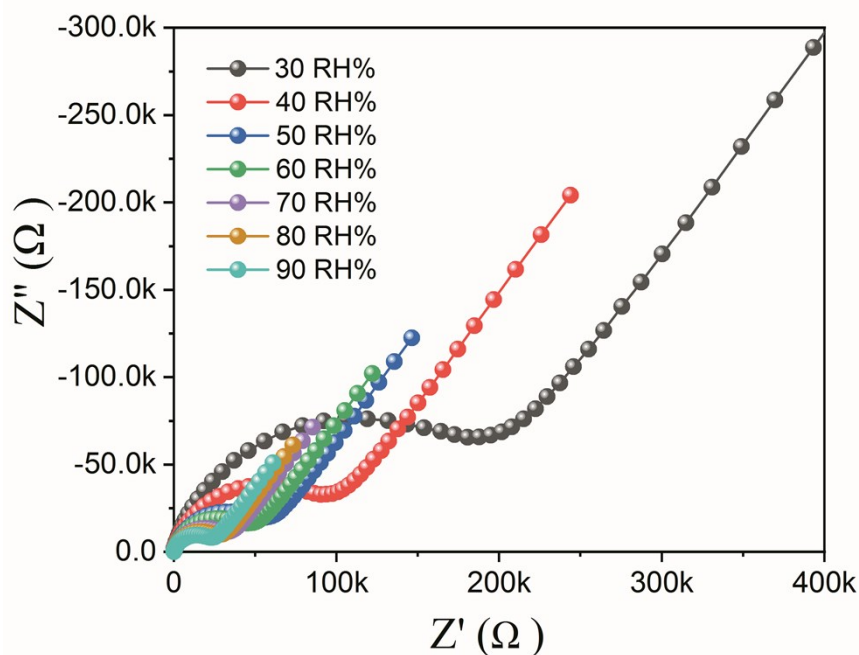


Fig. S13 Typical Nyquist plots of eHPW-PEI₁ at 25°C with different relative humidity.

The Nyquist plots of eHPW-PEI₁ at different humidity is shown in Fig. 13. Similar to most proton conductive materials, the proton conductivity of eHPW-PEI₁ increases with increasing humidity. This is because water molecules can participate in the construction of hydrogen bond networks and the transport of protons. The proton conductivity of eHPW-PEI₁ is $3.8 \times 10^{-4} \text{ S cm}^{-1}$ at 30 RH%, and reaches $3.3 \times 10^{-4} \text{ S cm}^{-1}$ at 90 RH%. The proton conductivity has increased by nearly 10 times, but the change of eHPW-PEI₁ proton conductivity with humidity is at a low level among proton conductive materials. Therefore, we believe that eHPW-PEI₁ is less dependent on humidity, which will facilitate its proton transmission in low humidity or high temperature environments. We believe that the good water retention and hydrophilicity of PVP enable the material to absorb more water molecules even in a low-humidity environment.